Influence of multiple scattering on the Coulomb-explosion imaging of fast molecules

D. Zajfman,* T. Graber,† E. P. Kanter, and Z. Vager‡
Physics Division, Argonne National Laboratory, Argonne, Illinois 60439
(Received 31 January 1992)

A quantitative analysis of the influence of small-angle multiple scattering on fast molecules dissociating in solids is made using a Monte Carlo technique. Simulations allow the computation of asymptotic velocities of all of the fragments after Coulomb explosion. It is found that only the simultaneous treatment of the Coulomb explosion and the multiple scattering leads to satisfactory agreement of the simulations with experimental data. Limits on the range of validity for Coulomb-explosion-imaging experiments are determined. It is shown that these limits are ample to allow quantitative spectroscopic data to be extracted from such experiments.

PACS number(s): 34.10.+x, 35.20.Dp

I. INTRODUCTION

Recent studies of the foil-induced dissociation of fast (MeV) molecular ions have demonstrated an alternative approach to the problem of determining the geometrical structures of molecular ions [1]. In these so-called "Coulomb-explosion-imaging" (CEI) experiments, a well-collimated beam of molecular ions strikes a thin target foil ($\sim 50-100$ Å). As a result, the valence electrons of the molecule are stripped away very rapidly ($<10^{-16}$ s) and the different constituent nuclei repel each other due to the mutual Coulomb forces. By measuring, with very high accuracy, the relative asymptotic momenta of the atomic fragments (as well as their charge states) one can, in principle, determine the internuclear geometry preceding the dissociation for *every* molecule in the beam.

While early work concentrated on measuring mean geometry [2–5], more recent Coulomb-explosion experiments are now aimed at studying the nuclear vibrations within polyatomic molecular ions [6,7]. This has necessitated the development of ultrathin stripper foils [8]. Ultrathin targets offer several advantages in such experiments. Among them, the decrease of all ion-solid interaction effects due to the relatively short dwell time of the projectiles in the target ($\sim 10^{-16}$ s) is of prime importance. These interactions between the molecular ion and the target can smear the final velocities of the molecular fragments, and thereby reduce the ability of such experiments to determine vibrational amplitudes. Such effects include the electronic polarization of the solid, the energy loss, the charge-state fluctuations of the dissociation fragments while in the target, and small-angle multiple scattering. Previous calculations [9] have shown that of these, the most important limiting factor for CEI experiments is the multiple scattering. While the initial distribution of internuclear distances in the molecule produces a distribution of final velocities, the multiple scattering can mimic the vibrational motions and thus must be deconvoluted from the measured distributions. Since these calculations [9] were limited to the case of diatomic molecules oriented perpendicular to the direction of the beam, they were not generally useful for deconvoluting the multiple scattering from the data.

The purpose of this work is to introduce a more complete calculation of multiple scattering of fast polyatomic molecules using a Monte Carlo simulation which treats the multiple scattering of the nuclei simultaneously with the Coulomb-explosion process. The characteristics of the multiple-scattering distributions for different target thicknesses, beam energies, molecular masses, and geometries are presented. From these results, the limits on the domain of applicability of the CEI method are explored.

II. COULOMB-EXPLOSION IMAGING

In a typical CEI experiment, for a molecule containing N atoms, measurements of the $3N$ velocity components after the explosion provides information on the $3N$ spatial components within the original molecule. We call these velocities the "V-space" coordinates while the original coordinates (internuclear distances and angles) are called "R-space" coordinates. These measured V-space coordinate distributions can, in principle, be directly related to the corresponding R-space coordinate distributions describing the fully correlated spatial geometry of the nuclei.

As an example, consider a diatomic molecule. If the equilibrium bond length is r_e and the stretching frequency is ν, then in the harmonic approximation the wave function of the ground vibrational state is given by

$$\Psi(r)=N_0 \exp[-(r-r_e)^2/(2\sigma_r^2)] , \quad (1)$$

where N_0 is a normalization factor and σ_r is given by

$$\sigma_r=\sqrt{\hbar/\mu\omega} , \quad (2)$$

where $\omega=2\pi\nu$ and μ is the reduced mass of the molecule.

In a CEI experiment, since all the asymptotic velocities after the Coulomb explosion are measured, the final kinetic energy distribution $G(E_k)$ of the fragments in the center of mass (i.e., in the frame of reference of the beam) can be extracted. This distribution is related to the initial internuclear distance distribution by

$$G(E_k)=|\Psi(r)|^2\frac{dr}{dE_k} . \quad (3)$$

The most probable value of the kinetic-energy distribution $E_{k,0}$ can be calculated by taking the derivative of Eq. (3). To first order in σ_r/r_e, and neglecting all ion-solid interactions as well as the minor initial internal kinetic energy due to vibrations, the most probable value of the final kinetic energy $E_{k,0}$ is simply given by

$$E_{k,0}=\frac{Q_2Q_2e^2}{r_e} , \quad (4)$$

where Q_1 and Q_2 are the final charge states of the two fragments. The width (i.e., the standard deviation) of the final kinetic-energy distribution due to the initial bond-length distribution (with a rms width given by $\sigma_r/\sqrt{2}$) can be evaluated by differentiating Eq. (4),

$$\sigma_E=\frac{Q_1Q_2e^2}{r_e^2}\frac{\sigma_r}{\sqrt{2}}=\frac{E_{k,0}^2}{Q_1Q_2e^2}\frac{\sigma_r}{\sqrt{2}} . \quad (5)$$

Thus, by measuring the final kinetic-energy distribution, the initial vibrational frequency can be deduced by combining Eqs. (2) and (5),

$$\omega=\frac{\hbar}{\mu}\left[\frac{E_{k,0}^2}{2Q_1Q_2e^2\sigma_E}\right]^2 . \quad (6)$$

It needs to be stressed that the result given by Eq. (6) is valid only if all ion-solid interactions are negligible. Another limitation is that the harmonic approximation has been used. Since the full energy distribution is measured, any anharmonicity present in the initial molecular potential will show up in the final kinetic energy as well. However, for the sake of simplification, we will continue to use this approximation.

As we have pointed out, the most important smearing effect for the final distribution is the multiple scattering. In Sec. IV we will present calculations done by computer simulations of the Coulomb-explosion process, of the contributions of the multiple scattering, and the charge fluctuations to the final width of the energy distribution and compare these for specific cases to the "natural width" given by Eq. (5).

III. COULOMB-EXPLOSION SIMULATION

The simulation is divided into two parts. First, the multiple scattering of each atom in a given molecule is generated individually for each of a given number of trajectories, typically of the order of 2000. The multiple-scattering computational procedure has been developed by Möller, Pospiech, and Schrieder [10], and its implementation has been described elsewhere [9,11,12]. This produces a list of scattering angles (polar and azimuthal), charge states, and time of each collision inside the target for each trajectory.

Then, for the case of molecular projectiles, in addition to this multiple scattering, the trajectories are modified by the mutual Coulomb repulsion between the fragments of the molecule, ignoring any possible correlations in the multiple scattering of the fragment ions. Early treatment of multiple scattering of Coulomb-exploding fragments assumed that the multiple scattering and the Coulomb repulsion are independent interactions producing additive small-angle deflections [13]. A model based on the Fokker-Planck equation to simultaneously incorporate these two effects previously demonstrated that important focusing and defocusing effects are not accounted for in the simpler model [14]. Moreover, it has been demonstrated that the interplay between multiple scattering and the Coulomb repulsion is orientation dependent [15]. For example, for a diatomic molecule with its internuclear axis aligned along the beam direction, the multiple-scattering deflections are perpendicular to the Coulomb-explosion forces, and we expect the dissociation process to be independent of the multiple scattering. However, for molecules aligned transverse to the beam directions, the Coulomb forces and the multiple-scattering affect the same velocity components and thus act "coherently."

The method of computation consisted of numerically integrating the equations of motion for the different "free paths" between each "collision" of any of the molecular fragments, as determined in the first part of the simulation, starting from an initial molecular geometry and a random orientation relative to the beam direction. At each collision, the velocity vector of the colliding atoms is rotated, as given by the polar and azimuthal angles computed in the first part of the simulation.

The Coulomb interaction between any two fragments, during the target dwell time, is modeled by a sum of screened pairwise potentials of the form

$$V_{ij}(r)=\frac{q_iq_je^2}{r_{ij}}e^{-r_{ij}/\alpha_t} , \quad (7)$$

where q_i and q_j are the instantaneous charges states of any pair of fragments during the "free path," and the exponential term reflects the screening due to target electrons. For slow projectiles, i.e., $v<v_0$ (v_0 is the Fermi velocity), the screening distance $\alpha_t=\alpha_s$ does not depend on the projectile velocity v and is always smaller than a typical internuclear distance (for example, $\alpha_s=0.4$ Å in carbon [16]). As a consequence, the Coulomb forces between fragments of a slow incident molecule are very weak within a solid medium. For projectiles with velocities $v>v_0$, one has to consider the effects of dynamic screening [17] in which $\alpha_t=\alpha_d$ is proportional to the cluster velocity and given by $\alpha_d=v/\omega_p$, where ω_p is the plasma frequency of the solid (for example, $\alpha_d=0.98$ Å for 2-MeV N_2^+ in carbon).

The result of this procedure produces the nuclear coordinates and velocities of each fragment at the exit of the target foil. Then the final velocities are calculated by computing the asymptotic trajectories of all fragments. Outside the target, the potential between any two fragments is assumed to have the form

$$U_{ij}(r)=\frac{\xi_i\xi_je^2}{r_{ij}}e^{-r_{ij}/\alpha_0}+\frac{Q_iQ_je^2}{r_{ij}}(1-e^{-r_{ij}/\alpha_0}) . \quad (8)$$

For light nuclei ($Z_i\leq 10$) α_0 is a constant (taken to be the

Bohr L-shell radius of the specific atom) which reflects the screening of any remaining L-shell electrons, and the ξ_i are defined as

$$\xi_i = \begin{cases} Z_i - 2 & \text{if } Q_i < Z_i - 2 \\ Q_i & \text{otherwise} \end{cases} \quad (9)$$

where the Z_i are the atomic numbers of the fragment nuclei. The first term in Eq. (8) reflects the complete screening of the nuclei by the K-shell electrons for internuclear separations smaller than α_0 but larger than the K-shell radius. In the case of $\xi_i = Q_i$, $U(r)$ is reduced to a pure Coulomb potential. Similar consideration can be used for heavier nuclei.

The final results of the simulation are the asymptotic velocities and charge states of each fragment. For the simulations reported here, the integration was stopped when the remaining potential energy in the system is lower than 2% of the potential energy at the exit of the target.

IV. RESULTS AND DISCUSSIONS

A. Diatomic molecules

We have computed the asymptotic distributions of kinetic energies in the center of mass (c.m.) for the Coulomb explosion of various diatomic molecules, as a function of beam energy and target thickness. As shown in Eq. (6), an important quantity of these distributions is the width σ_E which can be, when there is no multiple scattering, related to the initial vibrational frequency. A criterion to judge the importance of multiple scattering is the comparison of the width due to such scattering (σ_{MS}) to that caused by bond-length variations in the molecule due to zero-point vibrations (σ_E). Ideally, in order to be able to accurately deconvolute the natural width from the measured one, σ_{MS} should be smaller than σ_E.

As an example, Fig. 1 shows the simulated final kinetic-energy distribution (in the c.m.) for N_2^+ at three different beam energies: 1.5, 4.0, and 6.0 MeV for a target of Formvar with a thickness of 0.5 $\mu g/cm^2$ and final charge state $Q_1 = Q_2 = 3$. The bond-length distribution was chosen to be a δ function with $r_e = 1.11642$ Å [18], so that the final width shown in Fig. 1 is *only* due to the multiple scattering and charge fluctuations in the solid target. It is clear that the width of these distributions increases as the energy decreases, but most important are the long tails on the high-energy side. These tails are a result of the rotational kinetic energy which is pumped into the system due to the multiple scattering [19].

Figure 2 shows the comparison between the experimental results and simulation for a beam of N_2^+ at 2 MeV through a 2.5-$\mu g/cm^2$ Formvar target. In the experiment, the N_2^+ molecules were prepared in the ground state using a supersonic expansion source [20] located in the high-voltage terminal of the 5-MV Dynamitron at Argonne National Laboratory and measured using a specialized detector [21]. In the calculation, the initial bond-length distribution of the vibrational ground state [18] was included in the simulation, and the final charge states are $Q_1 = Q_2 = 2$. The agreement between the calculations and the experiment is excellent, including the high-energy tail which is also present in the experimental result. It should be pointed out that at such energy and target thickness, the multiple-scattering contribution σ_{MS} is much larger than σ_E so that the agreement between the simulation and the experiment in this case does not prove that the molecule was necessarily in the ground vibrational state. Figure 2 also shows, for comparison, the result of the simulation when the multiple scattering and the Coulomb repulsion are not treated simultaneously. In this case, the Coulomb explosion was

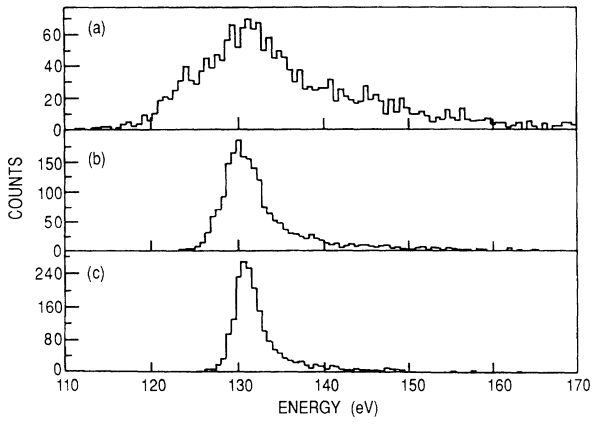

FIG. 1. Simulated final kinetic-energy distribution for N_2^+ at three different beam energies (a) 1.5 MeV, (b) 4 MeV, (c) 6 MeV. The target was 0.5-$\mu g/cm^2$ Formvar and the final charge states $Q_1 = Q_2 = 3$.

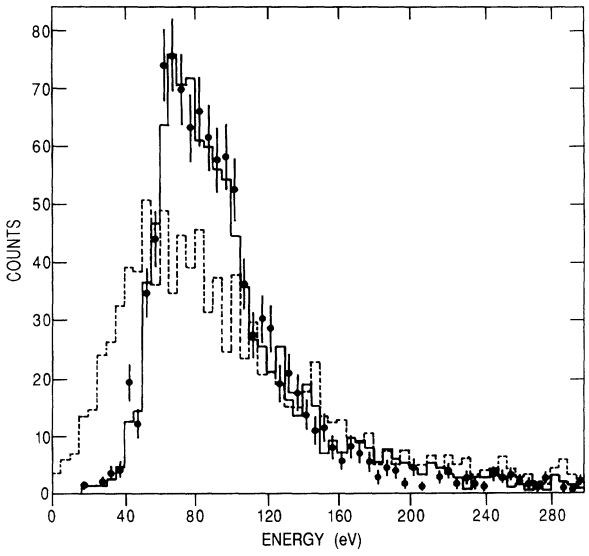

FIG. 2. Experimental (points with error bars) and simulated (solid line) kinetic-energy distributions for N_2^+ at 2 MeV through a 2.5-$\mu g/cm^2$ target. The final charge states are $Q_1 = Q_2 = 2$. The dashed curve represents the result of the simulation when the Coulomb repulsion and the multiple scattering are treated as independent processes (see text).

computed first without multiple scattering, and then the final nuclei velocities were smeared by an amount which was taken from the multiple scattering of a monoatomic beam using the previous simulation. Clearly, the treatment of "coherent" multiple scattering is important in this case and generates a narrower distribution than the incoherent, as was already proven by Sigmund [15].

In order to systematically quantify the widths of these distributions, we have fitted Gaussian functions to the central parts of the kinetic-energy distributions, neglecting the tails, and used the standard deviation of such fits to describe the widths. In Fig. 3, the standard deviations (σ_{MS}) of the final kinetic energies, due to multiple scattering (i.e., for a δ function initial R distribution), are shown as a function of beam energy for different target thicknesses for He_2^+ ($Q_1=Q_2=2$) and N_2^+ ($Q_1Q_2=3$) projectiles. The horizontal dashed lines in Fig. 3 correspond to the natural widths which would be expected for a "pure" Coulomb explosion of the vibrational ground state, i.e., calculated using Eqs. (2) and (5) and frequencies deduced from spectroscopic data. The energy range has been chosen so that it matches the capabilities of the different accelerators currently used for CEI experiments (i.e., the 5-MV Dynamitron at Argonne National Laboratory and the 12-MV Pelletron at the Weizmann Institute). Below about 4 MeV, the general trend is that σ_{MS} is decreasing strongly when the energy increases. For higher energies, the width is more or less independent of the energy, and remains at a constant level determined by target thickness. This is due to the fact that at high enough energy, the width due to the charge fluctuations inside the target (which lead to fluctuations in the effective internuclear potential) is larger than the contribution due to multiple scattering. The curve for N_2^+ corresponding to the thickest target (1.5 μg/cm^2) even tends to increase at high energy (above 8 MeV). This behavior can be understood using the following argument: Since all the curves are drawn for the same final charge state ($Q_1=Q_2=3$), at high energy in a thick target, these charge states are in the tail of the final charge-state distribution. Thus, charge-state fluctuations inside the target leading to such charge states are larger than when the final charge state is close to the most probable one. In order to check this, we carried out the same simulation for a target of 1.5 μg/cm^2, but computing only the trajectories leading to a final charge of $Q_1=Q_2=5$ on each nitrogen. The result is shown in Fig. 4 together with the previous result for $Q_1=Q_2=3$. It can be seen that the σ_{MS} is smaller for $Q_i=5$ than for $Q_i=3$ at high energy and larger at low energy, in agreement with the previous argument. The crossing around 10 MeV represents the energy where the intermediate ($Q_i=4$) charge is the most probable. For comparison, the width of the distribution for $Q_i=4$ is plotted on the same figure. It is important to point out that at these energies and target thickness, the charge-state distribution is not yet equilibrated. It is clear that this charge-state effect does not occur for light molecules (such as He_2^+) where the fluctuation of the charge states cannot be as large, and, furthermore, the final charge which has been chosen ($Q_i=Z_i=2$) is the most probable over the entire range of energies considered. It is thus important for minimizing multiple-scattering effects in CEI results that such experiments with nonequilibrated ions always consider the most probable charge state.

Figure 5 shows the widths of the simulated kinetic-

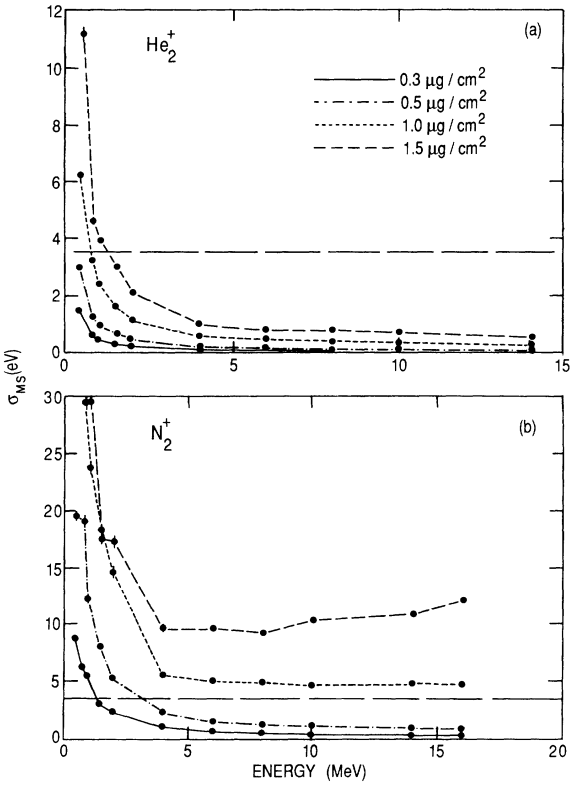

FIG. 3. Standard deviation of the simulated final kinetic energy for (a) He_2^+ and (b) N_2^+ as a function of beam energy for different target thicknesses assuming a fixed initial bond length. The horizontal dashed line is the vibrational contribution (σ_E), neglecting all foil effects, as given by Eq. (5).

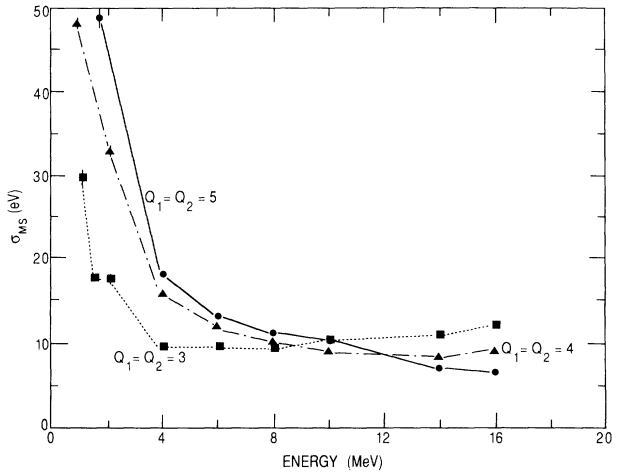

FIG. 4. Standard deviation of the simulated final kinetic energy for N_2^+ as a function of beam energy for different final charge states. The target thickness is 1.5 μg/cm^2.

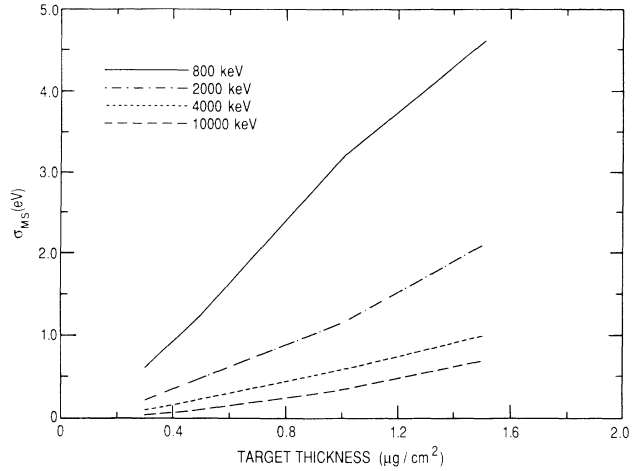

FIG. 5. Standard deviation of the simulated final kinetic energy as a function of target thicknesses for different beam energies for He_2^+.

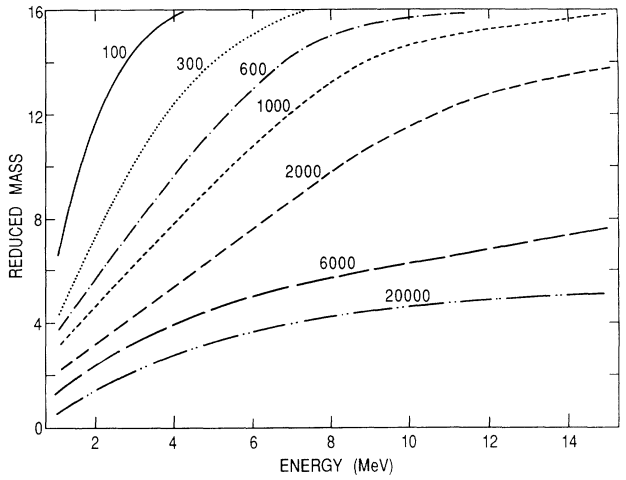

FIG. 7. Contour levels of the upper frequency limit for which the multiple scattering and the natural width are equal, as a function of both the reduced mass of the molecules and the beam energy for a 1-μg/cm^2 Formvar target. The frequencies on the different contours are in units of cm^{-1} and have been calculated from the widths of the simulated kinetic-energy distributions using Eq. (6).

energy distributions as a function of target thickness for He_2^+ at different beam energies. The dependence is generally linear. Shown in Fig. 6 is the width as a function of the molecular mass at constant energy and target thickness for the most probable charge state.

In order to condense these results in a useful way, we could try to answer the following question: Given a specific molecule, what is the domain of vibrational frequency for which the CEI technique will be a sensitive tool? The answer to that question can be deduced from Fig. 7. In this figure are displayed various contour levels corresponding to vibrational frequencies. The contours are shown as a function of the reduced mass of the molecule and its energy. Each contour represents the relation between the reduced mass and the energy for which the multiple-scattering width is equal to the natural width. They have been computed by estimating the widths of various simulated kinetic-energy distributions for different molecules and beam energies, and transforming these widths, with the aid of Eq. (6), to frequencies. The simulations were made with δ functions for the initial internuclear distributions and for a target thickness of 1.0 μg/cm^2. As such, they represent the contribution of the multiple-scattering and charge-changing process to the measured width. Since a *high* frequency corresponds to a *narrow* natural width, the numbers adjacent to each level represent the upper limit for the sensitivity of a CEI experiment for a given molecule at a given energy. These values can be easily scaled for various target thicknesses using Fig. 5 [and Eq. (6)]. As an example, using a molecular beam with a reduced mass of $\mu=8$ (such as O_2, for example) at 4.0 MeV, the upper limit on the frequency is about $\omega=800$ cm^{-1}. Doing the same experiment at an energy of 12 MeV will extend that limit to $\omega=5000$ cm^{-1}. It should be clear that these numbers represent only the fact that at these energies, the natural and multiple scattering widths are equal. This is not a fundamental limit since it is still possible to deconvolute the kinetic-energy spectrum. However, it is a practical limit since such deconvolution leads to increased experimental uncertainty.

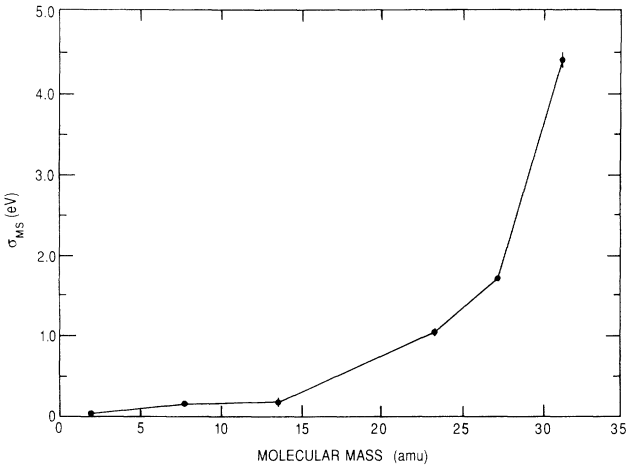

FIG. 6. Standard deviation of the simulated final kinetic energy as a function of the molecular mass for several diatomic projectiles. The beam energy is 4.5 MeV and the target thickness is 0.5 μg/cm^2.

Since the frequencies of most diatomic molecules are in the range of 1000 to 2000 cm^{-1}, it is clear that there is always a domain in which the width due to multiple scattering is smaller than the natural width due to zero-point vibrations. Since the thinnest Formvar targets which are practical are $\sim$0.5 μg/cm^2, it means that CEI experiments can be designed to be insensitive to such foil effects by choosing the right target thickness, energy, and charge state (i.e., the minimum energy being around 4

MeV for a target thickness of ~ 0.5 $\mu g/cm^2$, and the charge state being as close as possible to the most probable one). For relatively heavy systems ($\mu > 16$), higher energies than available with the present accelerators [both at Argonne (5 MV) and Weizmann (12 MV)] are needed in order to extract accurate bond-length distributions for ground-state molecules.

B. Polyatomic molecules

In the case of polyatomic molecules, it is less easy to extract general considerations though the procedure is straightforward. The analysis has to be carried out for many different vibrational modes. The effect of multiple scattering on vibrations involving mainly stretching between two atoms can easily be related to the diatomic case, but this is not true for bending (angular) motions. For such motions, it is expected that the multiple scattering and the Coulomb repulsion do not act coherently since for large bend angles, bending vibrations are mostly perpendicular to the strongest interatomic bonds (i.e., those with the largest Coulomb energies). On the other hand, the result will be very dependent upon the initial geometry of the molecule and focusing or defocusing effects can still occur.

In order to get a sense of how much the bending vibrational motion is affected by multiple scattering, we computed the final angular distribution of the two protons in the Coulomb explosion of H_2O^+. Figure 8 shows the distribution of the angle between the final velocities of each of the two protons relative to the oxygen fragment. The results shown are for three different energies (1.5, 4,0, and 6.0 MeV) with a target thickness of 1.0 $\mu g/cm^2$ and a final oxygen charge state $Q=4$. The initial bond angle was chosen to be $\theta_e = 108.4°$ and the O—H length $r_e = 0.997$ Å [7], each with δ function distributions. Thus, the width shown in Fig. 8 is due only to foil effects. Unlike the kinetic-energy distribution in Fig. 1, no asymmetries are apparent in the tails on either side of these distributions. Figure 9 shows the standard deviation ob-

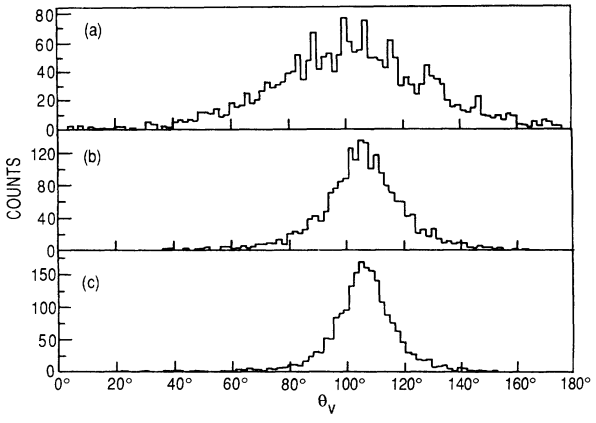

FIG. 8. Angular distribution between the final velocities of each of the two protons relative to the oxygen fragment for a beam of H_2O^+ through a 1-$\mu g/cm^2$ target at different energies: (a) 1.5 MeV, (b) 4.0 MeV, (c) 6.0 MeV. The final oxygen charge state is $Q=4$.

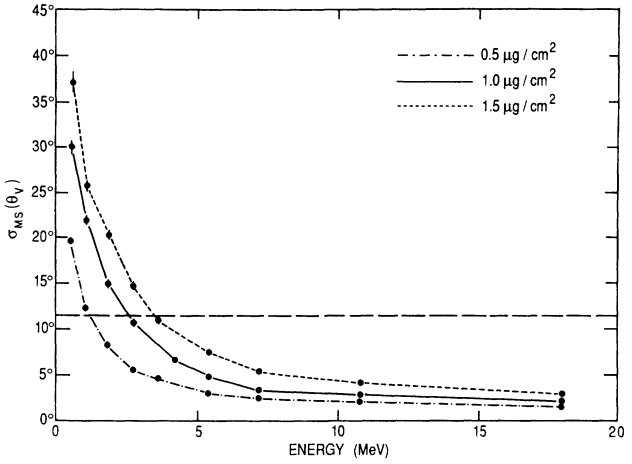

FIG. 9. Standard deviation of the V-space H-O-H angular distribution for H_2O^+ as a function of beam energy for different target thicknesses. The horizontal dashed line represents the natural width neglecting all foil effects.

tained by Gaussian fitting of the angular distribution for different target thicknesses as a function of the incident energy for a final charge state $Q=4$ on the oxygen. It has previously been experimentally demonstrated that the variations of the distributions for different charges states are relatively minor [7], since the final angle is only weakly influenced by the relative velocity between the protons and the oxygen and the H-H interaction is weaker than the O-H interaction. The width of the distribution σ_{MS} decreases strongly as the energy increases until about 4 MeV. Above that energy, σ_{MS} approaches a constant level, which is again due to the fluctuations of the charge inside the target. For comparison, the horizontal dashed line represents the natural width expected for a "pure" Coulomb explosion including zero-point vibrations. This line has been computed by running the simulation without any multiple scattering or charge fluctuations, but including an initial bond-length and bond-angle distribution [7] as given by standard spectroscopic data. Here again, for these thin foils, a CEI experiment can be relatively clean and the condition that the natural width has be larger than σ_{MS} can easily be achieved, even for this relatively stiff bending vibration.

V. CONCLUSIONS

The results of these simulations, and corresponding experiments, demonstrate that with ultrathin stripper foils (i.e., thinner than 1 $\mu g/cm^2$) and beam energies above 4 MeV, it is possible to deconvolute the multiple scattering from the results of CEI experiments, and thus measure the probability distribution of nuclei within molecules with relatively good precision [12]. An important factor is the vibrational frequency of the molecule which is analyzed. Here, we have considered only the zero-point motions of relatively stiff vibrations. Floppy molecules have very low frequencies, and consequently a large geometrical spread. Thus, the ratio between the width

due to foil effects and the natural width due to zero-point motion is much smaller than the cases considered here. Excited vibrational states in general also exhibit large amplitude motions and similar considerations apply to these. For such molecules, CEI can be quite a precise tool for obtaining structural information.

ACKNOWLEDGMENTS

The authors wish to thank Professor P. Sigmund for his helpful comments on this work. This work was supported by the U.S. Department of Energy, Office of Basic Energy Sciences, under Contract No. W-31-109-ENG-38.

---

*Present address: Department of Nuclear Physics, Weizmann Institute of Science, Rehovot, Israel.

†Also at Department of Physics, University of Illinois at Chicago, Chicago, IL 60680.

‡Also at Department of Nuclear Physics, Weizmann Institute of Science, Rehovot, Israel.

[1] Z. Vager, R. Naaman, and E. P. Kanter, Science **244**, 426 (1989).

[2] See, for example, D. S. Gemmell, Chem. Rev. **80**, 301 (1980), and references therein.

[3] Z. Vager, E. P. Kanter, G. Both, P. J. Cooney, A. Faibis, W. Koenig, B. J. Zabransky, and D. Zajfman, Phys. Rev. Lett. **57**, 2793 (1986).

[4] E. P. Kanter, Z. Vager, G. Both, and D. Zajfman, J. Chem. Phys. **85**, 7487 (1986).

[5] A. Belkacem, E. P. Kanter, R. E. Mitchell, Z. Vager, and B. J. Zabransky, Phys. Rev. Lett. **63**, 2555 (1989).

[6] D. Zajfman, E. P. Kanter, Z. Vager, and J. Zajfman, Phys. Rev. A **43**, 1608 (1991).

[7] D. Zajfman, A. Belkacem, T. Graber, E. P. Kanter, R. E. Mitchell, R. Naaman, Z. Vager, and B. J. Zabransky, J. Chem. Phys. **94**, 2543 (1991).

[8] G. Both, E. P. Kanter, Z. Vager, B. J. Zabransky, and D. Zajfman, Rev. Sci. Instrum. **58**, 424 (1987).

[9] D. Zajfman, G. Both, E. P. Kanter, and Z. Vager, Phys. Rev. A **41**, 2482 (1990).

[10] W. Möller, G. Pospiech, and G. Schrieder, Nucl. Instrum. Methods **130**, 265 (1975).

[11] D. Zajfman, Phys. Rev. A **42**, 5374 (1990).

[12] D. Zajfman, E. P. Kanter, T. Graber, Z. Vager, and R. Naaman, Nucl. Instrum. Methods B **67**, 22 (1992).

[13] Z. Vager and D. S. Gemmell, Phys. Rev. Lett. **37**, 1357 (1976).

[14] I. Plesser, Nucl. Instrum. Methods **194**, 269 (1982); Z. Vager, Ann. Israel Phys. Soc. **4**, 139 (1981).

[15] P. Sigmund, Nucl. Instrum. Methods B **67**, 11 (1992).

[16] J. Remillieux, Nucl. Instrum. Methods **170**, 31 (1980).

[17] N. Bohr, K. Dan. Vidensk. Selsk. Mat. Fys. Medd. **18**, No. 8 (1948).

[18] K. P. Huber and G. Herzberg, *Molecular Spectra and Molecular Structure* (Van Nostrand Reinhold, New York, 1979), Vol. 4.

[19] P. Sigmund (unpublished).

[20] T. Graber, D. Zajfman, E. P. Kanter, R. Naaman, Z. Vager, and B. J. Zabransky, Rev. Sci. Instrum. (to be published).

[21] A. Belkacem, A Faibis, E. P. Kanter, W. Koenig, R. E. Mitchell, Z. Vager, and B. J. Zabransky, Rev. Sci. Instrum. **61**, 946 (1990).